Sensors & Actuators: B. Chemical 307 (2020) 127655

Contents lists available at ScienceDirect

Sensors and Actuators B: Chemical

journal homepage: www.elsevier.com/locate/snb

Compact and planar type rapid response ppb-level SO_2 sensor based on stabilized zirconia and $SrMoO_4$ sensing electrode

Fangmeng Liu[a,*], Jing Wang[a], Li Jiang[a], Rui You[b], Qingji Wang[c], Caileng Wang[a], Zetian Lin[a], Zijie Yang[a], Junming He[a], Ao Liu[a], Peng Sun[a], Xu Yan[a], Geyu Lu[a,*]

[a] State Key Laboratory of Integrated Optoelectronics, Key Laboratory of Advanced Gas Sensors, Jilin Province, College of Electronic Science and Engineering, Jilin University, 2699 Qianjin Street, Changchun 130012, China
[b] Institute of Microelectronics, Peking University, Beijing 100871, China
[c] State Key Laboratory of Marine Resource Utilization in South China Sea, Hainan University, Haikou 570228, China

ARTICLE INFO

Keywords:
SO_2 sensor
ppb-level
$SrMoO_4$
Stabilized zirconia
Mixed-potential

ABSTRACT

The planar yttria-stabilized zirconia (YSZ) solid electrolyte based mixed potential type gas sensing devices attached with molybdate $MMoO_4$ (M: Ni, Co, Zn, Mn and Sr) sensing electrodes (SEs) were designed and fabricated, attempting to sensitively and rapidly monitor ppb-level SO_2. The sensor using $SrMoO_4$-SE possessed the highest potential response signal of -37.5 mV to 500 ppb SO_2 at 550 °C. More importantly, the low detection limit of 20 ppb SO_2 and fast response time of 37 s to 200 ppb SO_2 were presented for the device utilizing $SrMoO_4$-SE at 550 °C. The linear dependence between response value and the SO_2 concentration logarithm in the range of 0.02–1 ppm was observed, which the sensitivity (slop) was −29 mV/decade. Furthermore, the sensor also showed excellent selectivity, reproducibility and high temperature stability of 7 days to SO_2 at 550 °C. The mixed potential sensing mechanism was discussed and further verified based on the measurement of polarization curves.

1. Introduction

Sulfur dioxide (SO_2), as a representative harmful and hazardous air pollutant emission from fossil fuels and high temperature industrial processes, is responsible for formation of acid rain and photochemical smog. Additionally, the worry is that low ppm level or even ppb concentrations of SO_2 gas in air can also give rise to dysfunction of respiratory system, tissues and organ of human being, or even ultimately lead to death [1,2]. Therefore, *in-suit* real-time monitoring and precise measurement of SO_2 gas at the sources is critical to prevent environmental pollution and secure safety and health of human beings.

Currently, high precision instrument analysis technologies, such as gas chromatography and IR spectrum, have been widely used for analyzing and monitoring atmospheric pollutants. However, such huge, complex and extremely expensive detection instrument is difficult to use of future pollution detecting systems, especially high temperature *in-suit* detection system. Solid-state electrolyte type gas sensor based on mixed potential model has been viewed as the potential candidate for pollution gas detector due to its advantages of inexpensive, miniaturization, compatibility, easily integrated, mechanical and temperature stability. Up until now, different ambient pollution gases including NO_x, CO, NH_3, H_2S, C_xH_y, and VOCs have been primarily monitored for stabilized zirconia (YSZ)-based mixed potential type gas sensor based on various metal oxide sensing electrode materials [3–15]. For the mixed potential type gas sensor based on YSZ electrolyte, the suitable sensing material with high electrochemical catalytic activity plays a vital role in achieving good gas sensing performance. Fortunately, Lu et al. firstly proposed and developed YSZ-based mixed potential type electrochemical SO_2 sensor utilizing $MnNb_2O_6$ sensing electrode for monitoring sub-ppm level of SO_2 gas [16]. However, previous YSZ electrolyte type sensors do not show sensitive and fast detection ability of very low concentration of SO_2 with a single oxide sensing material. Thus, how to further design and prepare new composite oxide sensing electrode material for fabrication of high performance YSZ-based mixed potential type SO_2 sensor is also a valuable subject in the current research.

Herein, a compact and planar type stabilized zirconia based electrochemical sensor utilizing $SrMoO_4$ sensing electrode for monitoring ppb-level SO_2 at high temperature is presented. The molybdate $MMoO_4$ (M: Ni, Co, Zn, Mn, Sr) composite materials are designed and selected to fabricate YSZ-based mixed potential type gas sensors. The sensor attached with $SrMoO_4$-SE possessed the best sensing response to SO_2 and

* Corresponding authors.
E-mail addresses: liufangmeng@jlu.edu.cn (F. Liu), lugy@jlu.edu.cn (G. Lu).

https://doi.org/10.1016/j.snb.2020.127655
Received 6 August 2019; Received in revised form 18 December 2019; Accepted 2 January 2020
Available online 03 January 2020
0925-4005/

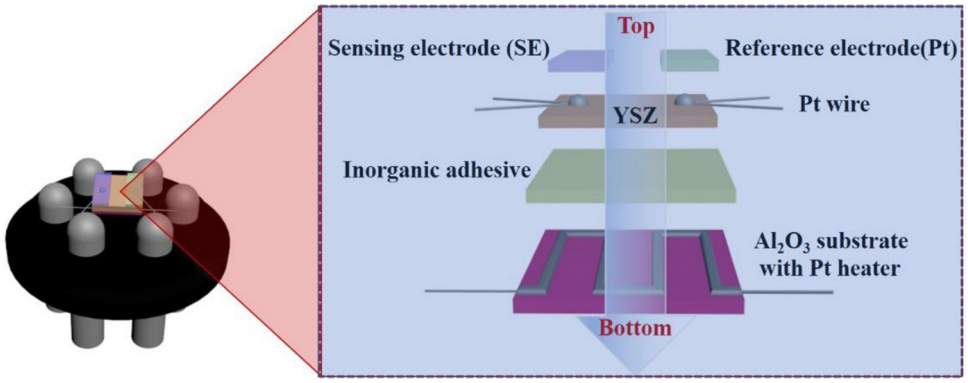

Fig. 1. Schematic diagram of designed sensor.

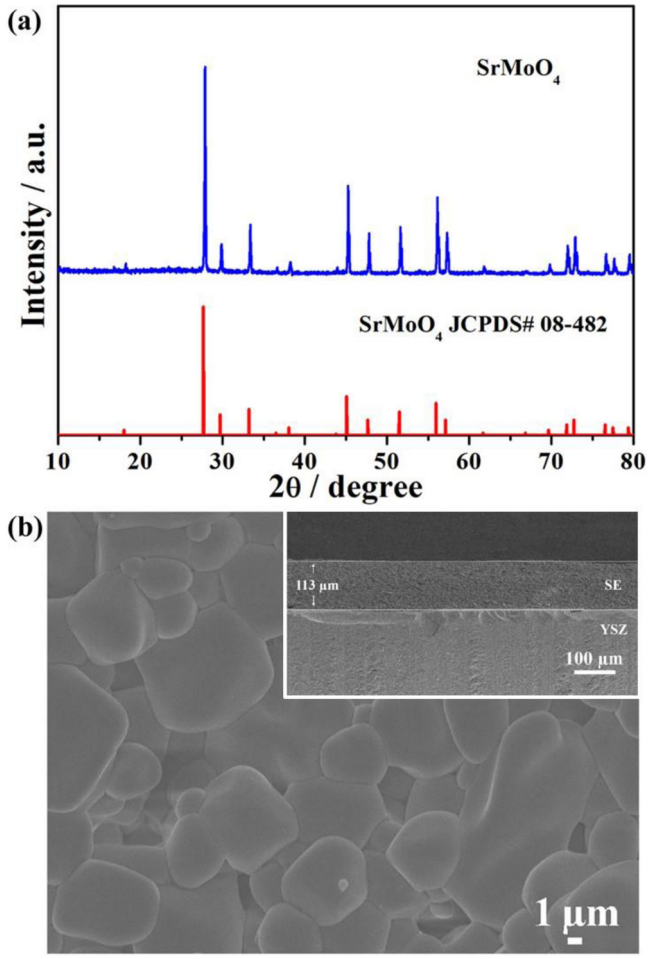

Fig. 2. (a) X-ray diffraction spectrum of $SrMoO_4$ sample; (b) Surface and cross-section (inset) SEM images of $SrMoO_4$ sensing electrode sintered at 800 °C.

the gas-sensing performance for the present device was systematically investigated and sensing mechanism was also discussed. It is noteworthy that the present work is the first successful attempt at fast and sensitively monitoring ppb-level SO_2 for YSZ-based mixed potential type sensor with a single $SrMoO_4$ composite oxide electrode.

2. Experimental

The $SrMoO_4$ sensing material was prepared using a facile sol-gel method as reported [17]. The sensor was designed based on the YSZ plate (8 mol% Y_2O_3-doped, 2 mm × 2 mm square, 0.3 mm thickness, provided by Anpeisheng Corp., China), molybdate $MMoO_4$ (M: Ni, Co, Zn, Mn and Sr) sensing electrode materials, Pt paste (Sino-platinum Metals Co., Ltd.), Pt wire (Diameter of 0.05 mm, purchasing from Sino-platinum Metals Co., Ltd.), inorganic adhesive and Al_2O_3 substrate with Pt heater (Length × Width × Thickness: 2 mm × 2 mm × 0.2 mm, providing the working temperature for the device), which references to our previous fabrication process [5,7]. Finally, YSZ-based sensing devices based on different sensing electrodes were sintered at 800 °C for 2 h in muffle furnace. The schematic diagram of the fabricated sensor is depicted in Fig. 1.

X-ray diffraction (XRD) patterns of $SrMoO_4$ sensing material was performed using a Rigaku wide-angle X-ray diffractometer (D/max rA, using Cu Kα radiation at wave length =0.1541 nm) in the 2θ range from 10 to 80° with 0.02°/min. The field-emission scanning electron microscopy (FESEM, JEOL JSM-7500 F, with an accelerating voltage of 15 kV) were used to study surface morphology and microstructure of SE. Raman spectroscopy of $SrMoO_4$ sensing material was operated on LabRAM HR Evolution spectrometer with a laser wavelength of 532 nm. X-ray photoelectron spectroscopy (XPS) was performed using a Thermo ESCALAB250 spectrometer equipped with an Al-Kα ray source to obtain the composition information of $SrMoO_4$. The potential difference (V) between the SE and the RE was measured using a digital electrometer (Rigol. DM3054) when the sensor was placed in various gases or air based on static test system. The detailed sensing process follows to test procedures: The different concentrations of SO_2 gas is obtained in 1 L of airtight chamber by mixing different volume of standard SO_2 gas and air. The developed gas sensor is placed in airtight chamber with air or different concentrations of tested gases. Firstly, the airtight chamber is filled by pure air using an air pump. Then, a certain amount of SO_2 standard gas is injected into the chamber via a special airlock at side of the chamber using a microsyringe and make the test gases distribute uniformly in the chamber. Similar gas sensing measurement process is performed in other tested gases. The polarization curves of sensor were carried out utilizing the electrochemical workstation (CHI600C, Instrument corporation of Shanghai, China) in air and the different concentration of SO_2 gas (0.2 ppm, 0.5 ppm and 1 ppm SO_2 + air) at 550 °C. The complex impedance measurements of the developed devices were performed using impedance analyzer (Solartron 1260 and Solartron 1287) in different tested gases at 550 °C.

3. Results and discussion

XRD pattern of $SrMoO_4$ calcinated at 800 °C is presented in Fig. 2**(a)**. It is clear that all of diffraction peaks of prepared sample can be readily indexed to the scheelite-type tetragonal structure of $SrMoO_4$ with *I*41/a space group, which is matched well with the standard JCPDF card No. 08-0482. No impurity diffraction peaks were observed, indicating that the single phase of $SrMoO_4$ were formed. The sharp diffraction peaks suggested good crystalline nature. The surface

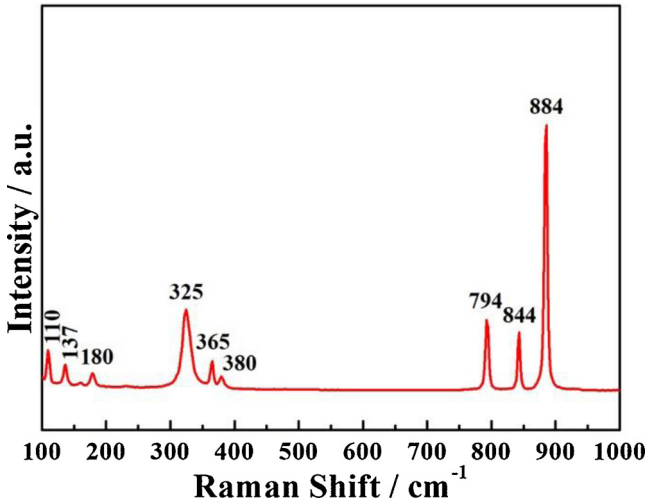

Fig. 3. Raman spectrum of $SrMoO_4$ sensing material.

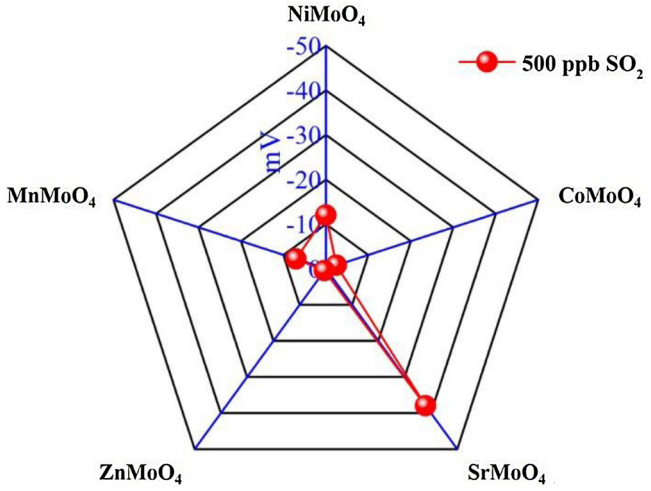

Fig. 5. Responses of the sensors using $MMoO_4$ (M: Ni, Co, Zn, Mn, Sr)-SEs to 500 ppb SO_2.

morphology of $SrMoO_4$ sensing electrode sintered at 800 °C was characterized by FESEM, as shown in Fig. 2**(b)**. The porous structure of $SrMoO_4$, packed by micrometer-sized particle, was observed. Clearly, the thickness of the sensing electrode is approximately 113 μm, (inset of Fig. 2**(b)**).

Fig. 3 depicts Raman spectrum of $SrMoO_4$ sensing material. The Raman diffraction peaks at 110 cm^{-1} and 137 cm^{-1} were related to the external vibrations due to the motion between Sr^{2+} cations and $[MoO_4]^{2-}$ tetrahedra [18]. Further, the Raman peak at 180 cm^{-1} was specified as free rotation mode of υ_{fr} (F_1). The diffraction peaks at 325 cm^{-1}, 365 cm^{-1} and 380 cm^{-1} observed in the wavenumber region of 250–450 cm^{-1} corresponds to the internal bending vibrational modes of υ_2 (A_g) and υ_4 (B_g), and the internal stretching vibration modes of υ_1 (A_g), υ_3 (B_g) and υ_3 (E_g) for $[MoO_4]^{2-}$ tetrahedra were observed at 884 cm^{-1}, 844 cm^{-1} and 794 cm^{-1}, respectively [19,20]. No other impurity diffraction peaks were observed in the XRD or Raman spectra of prepared sample. Therefore, it is reasonable to believe that well-crystallized $SrMoO_4$ sensing electrode material have been successfully prepared in this work.

The XPS measurement was used to analyze the chemical bonding state of elements in $SrMoO_4$ sensing material calcinated at 800 °C. Fig. 4**(a)** shows XPS spectrum of Sr 3d in $SrMoO_4$ with a core binding energy of 132.4 eV for $3d_{5/3}$ and 134.1 eV for $3d_{3/2}$, representing the characteristic of Sr^{2+} [21]. The binding energy peaks at 231.8 eV and 234.9 eV observed in Mo 3d (Fig. 4**(b)**) are attributed to Mo $3d_{5/2}$ and Mo $3d_{3/2}$, respectively. The binding energy peaks and the splitting width of 3.1 eV between Mo $3d_{3/2}$ and Mo $3d_{5/2}$ are in good agreement with those reported for Mo^{6+} [22].

To appraise the gas sensing properties of different molybdate composite oxide materials, such as $SrMoO_4$, $NiMoO_4$, $CoMoO_4$, $ZnMoO_4$ and $MnMoO_4$, the response of sensors combining $MMoO_4$ (M: Sr, Ni, Co, Zn and Mn)-SEs to 500 ppb SO_2 was measured and demonstrated in Fig. 5. Remarkably, among five sensing devices, the undoubtedly highest response signal of −38 mV to 500 ppb SO_2 was observed for the device attached with $SrMoO_4$-SE, indicating that $SrMoO_4$ in different developed molybdate is the optimal potential candidate electrode material of YSZ-based mixed potential type SO_2 sensor. Accordingly, the systematic investigation on sensing performance of the sensor attached with $SrMoO_4$-SE was performed in the following section. As reported previously, the sensing response of the sensor was affected by the operating temperature. Temperature dependence curves of the sensor attached with $SrMoO_4$-SE to 1 ppm SO_2 at 450 °C–575 °C were measured and shown in Fig. 6**(a)**. The response potential of the sensor attached with $SrMoO_4$-SE to 1 ppm SO_2 in the operating temperature range of 450 °C–550 °C increased gradually with increase of working temperature. The tendency of increasing sensing property is mainly attributed to enhanced electrochemical reaction activation degree of SO_2 at interface of stabilized zirconia and $SrMoO_4$ sensing electrode. Furthermore, the response and recovery speeds are accelerated in the

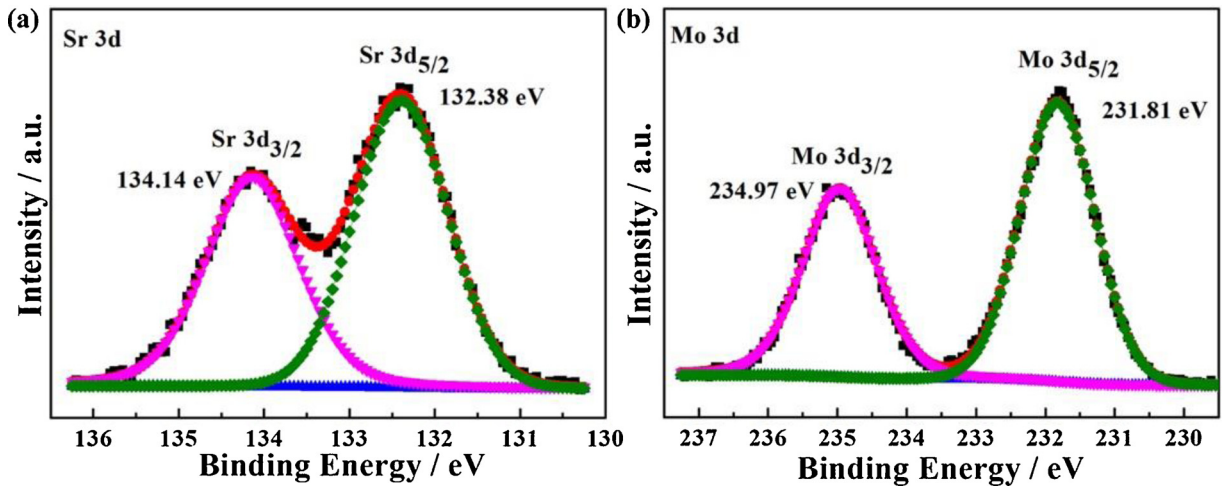

Fig. 4. XPS spectra of $SrMoO_4$ sensing material (a) Sr 3d and (b) Mo 3d.

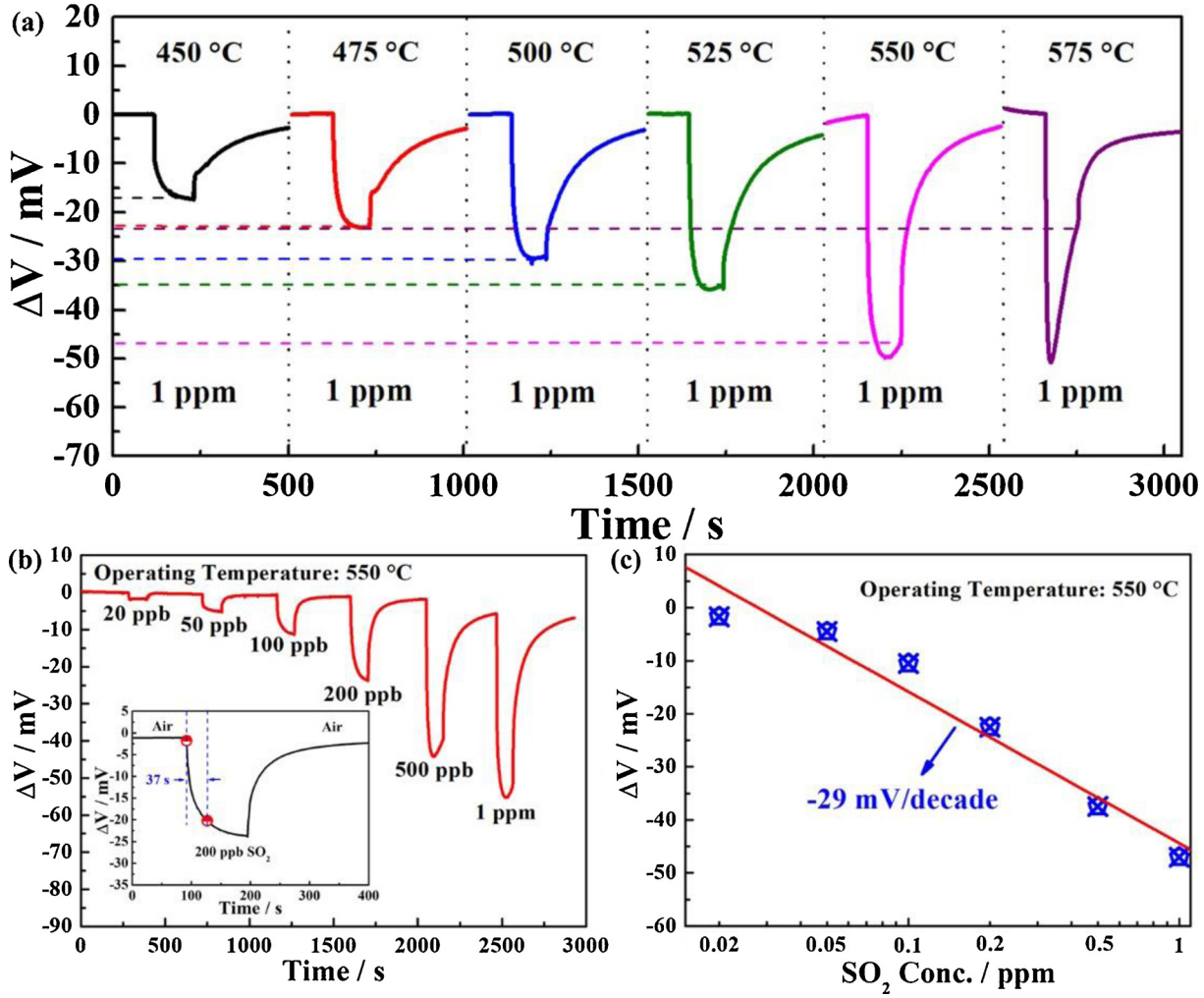

Fig. 6. (a) Temperature dependence curves of the sensor attached with $SrMoO_4$-SE to 1 ppm SO_2; (b) Dynamic response and recovery curves for the sensor using $SrMoO_4$-SE to 20 ppb-1 ppm SO_2 at 550 °C; (c) Dependence relation between sensing response and SO_2 concentration range of 20 ppb to 1 ppm.

temperature-rise process, due to the enhanced gas diffusion speed in the sensing electrode layer is conducive to shorten the time of arriving to triple phase boundary (TPB) of YSZ-Gas-SE. When the operating temperature is higher than 550 °C, the response potential presented the trend of increase-maximum-decrease and the response value of the sensor to 1 ppm SO_2 was lower than that of the operating temperature of 550 °C. The sharp spike potential signal is observed at 575 °C is mostly related to the desorption-dominant process because of the excessive operating temperature. Therefore, the operating temperature of 550 °C is appointed to optimal working temperature of the developed sensor and the relevant sensing property of the sensor utilizing $SrMoO_4$-SE is performed at 550 °C. Fig. 6**(b)** depicts the dynamic response and recovery curves for the sensor using $SrMoO_4$-SE to 20 ppb - 1 ppm SO_2 at 550 °C, the response potential signal of the sensor enhanced gradually with increase of tested SO_2 concentration at 550 °C. The sensor utilizing $SrMoO_4$-SE exhibited the response value of −22.5 mV and 90 % response time of 37 s to 200 ppb SO_2 at 550 °C. More importantly, the low detection limit of 20 ppb SO_2 was measured and obtained for the developed sensor, which represents the detection ability of low concentration SO_2. The potential response was negative linear relation to logarithm of SO_2 concentration in the range of 0.02 − 1 ppm at 550 °C, which the sensitivity (slop) for the fabricated sensor to 0.02 − 1 ppm SO_2 was −29 mV/decade (Fig. 6**(c)**). By comparing the SO_2 sensing property of the sensors previously reported (Table 1), it can be firmly concluded that the fabricated device utilizing $SrMoO_4$-SE displays better sensing performance in terms of response value, response time, sensitivity and low detection limit, which demonstrates its promising prospect and important application value in detection of ppb-level SO_2.

The reproducibility of the sensor attached with $SrMoO_4$-SE in 200 ppb SO_2 at 550 °C is illustrated in Fig. 7**(a)**. It was clearly observed that the response value and response transients of the sensor presented good consistency in 7 cycles of 200 ppb SO_2 at 550 °C, which confirms good SO_2 reproducibility. Fig. 7**(b)** shows the selectivity of the sensor towards various tested gases. Here, the selectivity of sensors was measured by exposing them to 500 ppb SO_2, 500 ppb H_2S, 10,000 ppm CO_2 and 100 ppm of different gases including C_2H_4, NO_2, NH_3, CO, CH_4 and acetaldehyde at 550 °C. As can be seen, the sensor exhibited the highest response value to 500 ppb SO_2 comparing with other interference gases, elaborating the higher selectivity towards SO_2. The high temperature stability of the sensor is also an important evaluation parameter of YSZ-based gas sensor to determine its practical applications. Therefore, the response value fluctuation of the sensor to 100 ppb SO_2 and 500 ppb SO_2 in continuous measurement of 550 °C were performed as shown in Fig. 7**(c)**. It was clearly observed that the potential value of the sensor combining $SrMoO_4$-SE responded consistently with a slight increase/decrease to 100 ppb SO_2 and 500 ppb SO_2 in 7 days of continuous high temperature test period. In order to demonstrate quantitatively the deviation of potential response value with test time, the change of the response value ($\triangle V_s$) for the sensor is defined using $\triangle V_s = [(\Delta V_n - \Delta V_0)/\Delta V_0 \times 100\ \%]$ (ΔV_n and ΔV_0 denote the response value to SO_2 on the n and initial days). A deviation of 19 % and -19.7%–100 ppb SO_2 and 500 ppb SO_2 was observed, which confirms

Table 1
Summary of SO_2 sensing performance in this work and other reported YSZ-based mixed potential type devices.

Sensing Materials	SO_2 Conc. (ppm)	Response (mV)※	Sensitivity (mV/decade)※	Response time (s)	Low Detection Limit (ppb)	Ref.
$SrMoO_4$	0.2	22.5	29	37 (0.2 ppm)	20	This work
$MnNb_2O_6$	5	27	13	103 (0.2 ppm)	50	[16]
$ZnTiO_3$	1	22.5	23	117 (0.2 ppm)	100	[23]

※ Absolute value.

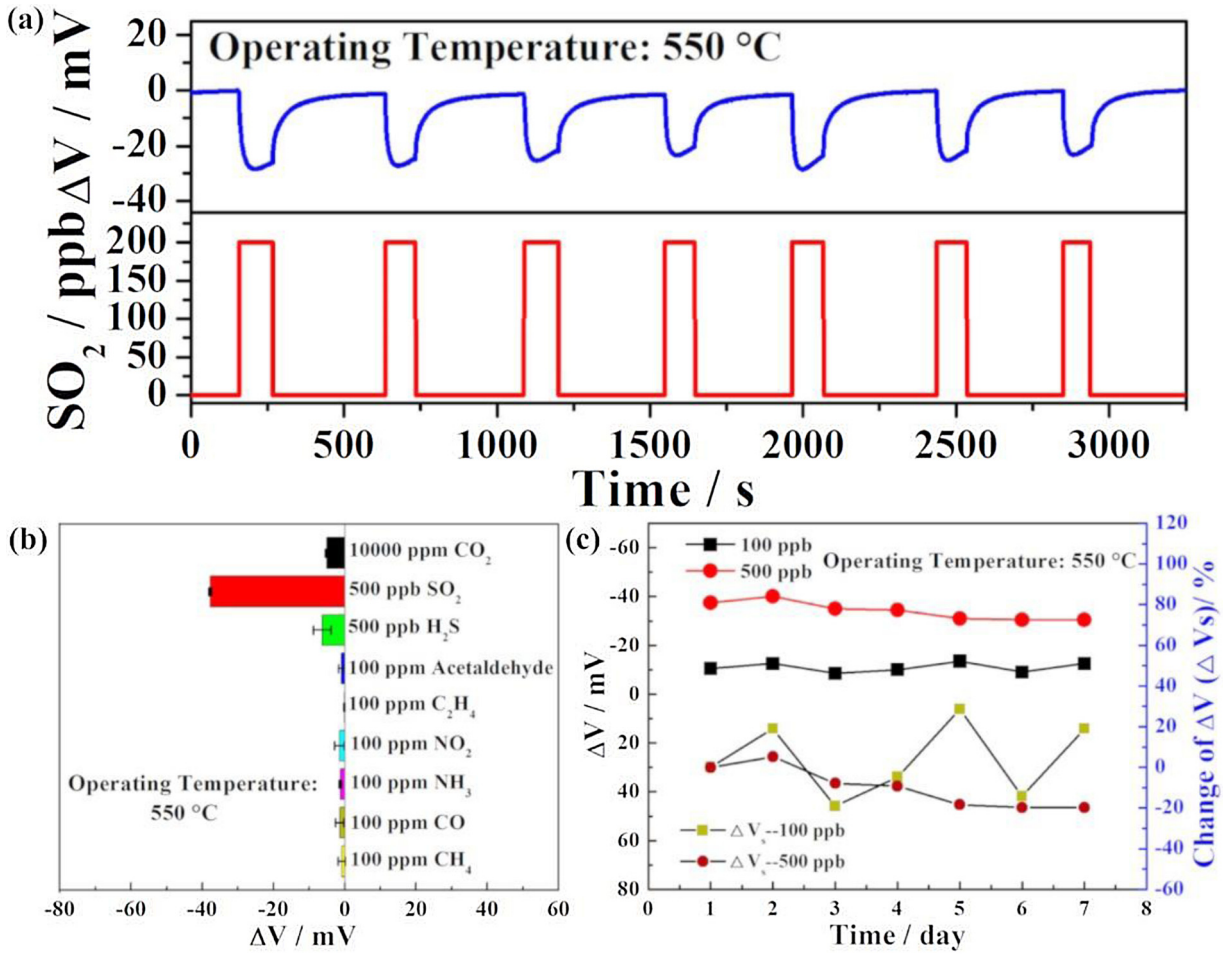

Fig. 7. (a) Reproducibility of the sensor attached with $SrMoO_4$-SE in 7 cycles of 200 ppb SO_2 at 550 °C; (b) Selectivity of the sensor to various gases; (c) High temperature stability of the sensing device in continuous measurement of 7 days.

good temperature stability.

To explain and verify the mixed potential sensing model for developed sensing device in this work, the polarization curves for the sensor attached with $SrMoO_4$-SE in air and different concentrations of SO_2 in the range of 200 ppb to 1 ppm were measured at 550 °C, as shown in Fig. 8. The cathodic polarization curve in air was measured. The modified anodic polarization curves in different concentrations of SO_2 were achieved by subtracting the current values in air from those obtained in SO_2 containing air. The intersection of the cathodic and modified anodic polarization curves was defined to estimated mixed potential. By comparing between the potential response values experimentally observed (−22.5 mV, −37.5 mV and −47 mV) for sensors attached with $SrMoO_4$-SE and the mixed potential estimated values (-25 mV, −35 mV and −44.5 mV) to 200 ppb SO_2, 500 ppb SO_2 and 1 ppm SO_2, both of them are in agreement well with each other. This result clearly indicating that the designed sensor conforms to the mixed-potential sensing mechanism [24,25].

The electrochemical cell of the fabricated sensor can be expressed in sample gas or base gas:

$$SO_2 + O_2 \text{ or } O_2, SrMoO_4/YSZ/Pt, SO_2 + O_2 \text{ or } O_2 \quad (1)$$

In sample gas ($SO_2 + O_2$), two competitive electrochemical reactions of anodic and cathodic occurred simultaneously at TPB of $SrMoO_4$/Electrolyte/sample gas on sensing electrode and the mixed potential was obtained at equilibrium, which is recorded in the response transients.

$$\text{Cathodic reaction: } O_2 + 4e^- \rightarrow 2O^{2-} \quad (2)$$

$$\text{Anodic reaction: } SO_2 + O^{2-} \rightarrow SO_3 + 2e\text{-} \quad (3)$$

Moreover, the gas-phase catalytic reaction of SO_2 ($SO_2 + O_2 \rightarrow SO_3$) in $SrMoO_4$ sensing layer results in the consumption of part SO_2. As depicted in Fig. 2**(b)**, the porous structure of $SrMoO_4$ sensing layer provide path to tested gas and is conducive to reduce the diffusion time and depletion of SO_2. In this regard, the more SO_2 gas reaches to the TPB participated directly in electrochemical reactions, which get good

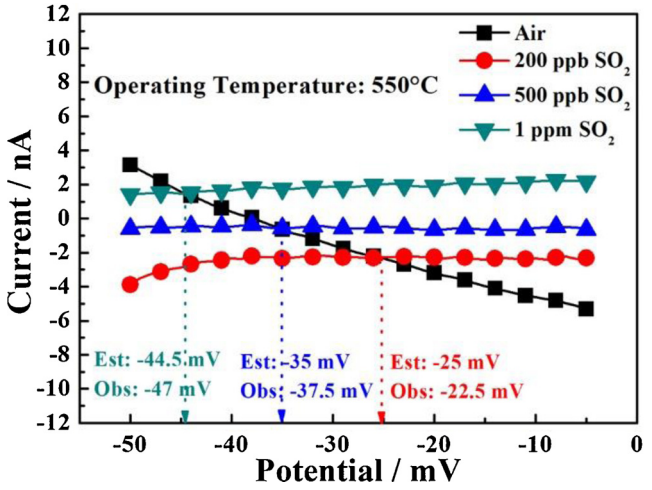

Fig. 8. Modified polarization curves for the sensor attached with $SrMoO_4$-SE in air, 200 ppb SO_2, 500 ppb SO_2 and 1 ppm SO_2 at 550 °C.

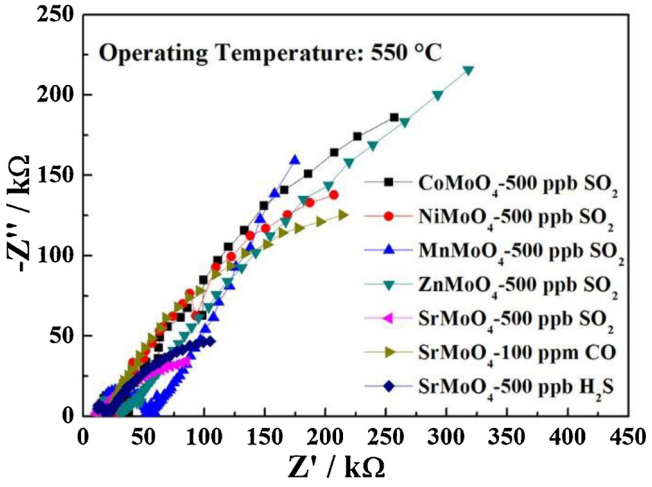

Fig. 9. Complex impedance curves for the sensors utilizing $MMoO_4$ (M: Ni, Co, Zn, Mn, Sr)-SEs in 500 ppb SO_2 and complex impedance curves of the device based on $SrMoO_4$-SE in different tested gases at 550 °C.

sensitivity. As the aforementioned result in Fig. 6**(c)**, the excellent linear relationship between response value and concentration logarithm of SO_2 can be explained by the mixed-potential sensing mechanism. The potential response of the sensor can be treated quantitatively according to Butler-Volmer Equation [26,27]. The mixed potential V_M can be represented by following Equation:

$$V_M = V_0 - nA \ln C_{SO_2} + mA \ln C_{O_2} \quad (4)$$

Clearly, from Eq. (5), the linear relationship between V_M and the logarithm of SO_2 concentration presents negative slope (-nA) under the fixed O_2 concentration, in accordance with experimental result of Fig. 6**(c)**. Above analysis further means that the sensor using $SrMoO_4$-SE follows the mixed potential model.

To further clearly explain and understand the sensing behavior for the fabricated sensors, the electrochemical impedance spectroscopy (EIS) of the sensors utilizing $MMoO_4$ (M: Ni, Co, Zn, Mn, Sr)-SEs in 500 ppb SO_2 were investigated at 550 °C, as depicted in Fig. 9. The semicircular region at high frequencies is normally attributed to the bulk resistance of YSZ electrolyte and SE, which is not affected by target gases. While the larger semicircle at low frequencies of approximately 0.1 HZ is considered to interfacial charge transfer characteristic of electron transfer-limited process between YSZ electrolyte and SE [28,29]. Noticeably, the fabricated sensor using $SrMoO_4$-SE showed the smallest semicircle both in high and low frequencies region, which indicated the highest electrochemical catalytic reaction activity to 500 ppb SO_2. In this case, the sensor attached with $SrMoO_4$-SE possessed the highest sensing performance to 500 ppb SO_2 at 550 °C. Similarly, to better elaborate good SO_2 selectivity of the device using $SrMoO_4$-SE, we continuous to investigate the electrochemical characteristics of the sensor in different interfering gases using EIS technology. Fig. 9 shows complex impedance curves of the sensor utilizing $SrMoO_4$-SE in 500 ppb SO_2, 500 ppb H_2S and 100 ppm CO at 550 °C. The developed sensing device showed the lowest interfacial resistance to 500 ppb SO_2 among the tested different gases, which demonstrated the highest electrochemical catalytic activity to SO_2. The sensor utilizing $SrMoO_4$-SE generates the best selectivity to SO_2 at 550 °C (Fig. 7**(b)**).

4. Conclusion

Briefly, an array of molybdate composite materials including $NiMoO_4$, $CoMoO_4$, $ZnMoO_4$, $MnMoO_4$ and $SrMoO_4$ were designed and were firstly used to prepare new compact and planar type YSZ-based mixed potential type gas sensors for monitoring ppb-level of SO_2 at high temperature. Results demonstrated that the sensor combining with $SrMoO_4$-SE possessed the highest potential response to 500 ppb SO_2 at 550 °C, which is mainly attributed to the largest electrochemical reaction degree at TPB. More importantly, the sensor utilizing $SrMoO_4$-SE also exhibited the low detection limit of 20 ppb SO_2, high sensitivity of −29 mV/decade in concentration range of 0.02 − 1 ppm, rapid response speed, excellent selectivity, good reproducibility and temperature stability at 550 °C. Good SO_2 sensing property presages that $SrMoO_4$ can be regarded as a promising candidate electrode material for YSZ-based ppb-level SO_2 sensor at high temperature.

Declaration of Competing Interest

The authors declare that they have no known competing financial interests or personal relationships that could have appeared to influence the work reported in this paper.

Acknowledgements

This work is supported by the National Nature Science Foundation of China (Nos. 61831011, 61803171, 61520106003, 61722305 and 61833006), Program for Chang Jiang Scholars and Innovative Research Team in University (No. IRT-17R47), National Key Research and Development Program of China (Nos. 2016YFC0207300 and 2016YFC0201002), Application and Basic Research of Jilin Province (20130102010 JC), Young Elite Scientists Sponsorship Program by CAST (2018QN RC001), Program for JLU Science and Technology Innovative Research Team (JLUSTIRT 2017TD-07), China Postdoctoral Science Foundation Funded Project (No.2018M630322, 2019T120239), Jilin Provincial Science and Technology Development Program (20190103155JH), Jilin Provincial Education Department Science and Technology Project (JJKH20190114KJ), Fundamental Research Funds for the Central Universities.

References

[1] J. Fergus, A review of electrolyte and electrode materials for high temperature electrochemical CO_2 and SO_2 gas sensors, Sens. Actuators B Chem. 134 (2008) 1034–1041.
[2] S. Lee, B. Hwang, S. Lee, H. Choi, S. Kim, S. Jung, D. Ragupathy, D. Lee, J. Kim, A novel tin oxide-based recoverable thick film SO_2 gas sensor promoted with magnesium and vanadium oxides, Sens. Actuators B Chem. 160 (2011) 1328–1334.
[3] A. Bhardwaj, I.-H. Kim, J.-W. Hong, A. Kumar, S.-J. Song, Transition metal oxide (Ni, Co, Fe)-tin oxide nanocomposite sensing electrodes for a mixed-potential based NO_2 sensor, Sens. Actuators B Chem. 284 (2019) 534–544.
[4] T. Ritter, G. Hagen, J. Kita, S. Wiegärtner, F. Schubert, R. Moos, Self-heated HTCC-based ceramic disc for mixed potential sensors and for direct conversion sensors for

automotive catalysts, Sens. Actuators B Chem. 248 (2017) 793–802.
[5] F. Liu, B. Wang, X. Yang, Y. Guan, R. Sun, Q. Wang, X. Liang, P. Sun, G. Lu, High-temperature stabilized zirconia-based sensors utilizing MNb_2O_6 (M: Co, Ni and Zn) sensing electrodes for detection of NO_2, Sens. Actuators B Chem. 232 (2016) 523–530.
[6] K. Mahendraprabhu, A. Sharma, P. Elumalai, CO sensing performances of YSZ-based sensor attached with sol-gel derived ZnO nanospheres, Sens. Actuators B Chem. 283 (2019) 842–847.
[7] F. Liu, R. Sun, Y. Guan, X. Cheng, H. Zhang, Y. Guan, X. Liang, P. Sun, G. Lu, Mixed-potential type NH_3 sensor based on stabilized zirconia and $Ni_3V_2O_8$ sensing electrode, Sens. Actuators B Chem. 210 (2015) 795–802.
[8] M. Khan, F. Qazi, Z. Hussain, M. Idrees, S. Soomro, S. Soomro, Recent trends in electrochemical detection of NH_3, H_2S and NO_x gases, Int. J. Electrochem. Sci. 12 (2017) 1711–1733.
[9] H. Jin, X. Zhang, C. Hua, X. Zhang, J. Zou, W. Shen, J. Jian, Further enhancement of the light-regulated mixed-potential signal with ZnO-based electrodes, Sens. Actuators B Chem. 255 (2018) 3516–3522.
[10] C. Wang, A. Liu, X. Yang, J. Wang, R. You, Z. Yang, J. He, L. Zhao, F. Liu, X. Yan, X. Liang, Y. Gao, F. Liu, P. Sun, G. Lu, YSZ-based mixed-potential type highly sensitive acetylene sensor based on porous SnO_2/Zn_2SnO_4 as sensing electrode, Sens. Actuators B Chem. 293 (2019) 166–172.
[11] L.-K. Tsui, A. Benavidez, P. Palanisamy, L. Evans, F. Garzon, Automatic signal decoding and sensor stability of a 3-electrode mixed-potential sensor for NO_x/NH_3 quantification, Electrochim. Acta 283 (2018) 141–148.
[12] F. Liu, Y. Guan, R. Sun, X. Liang, P. Sun, F. Liu, G. Lu, Mixed potential type acetone sensor using stabilized zirconia and $M_3V_2O_8$ (M: Zn, Co and Ni) sensing electrode, Sens. Actuators B Chem. 221 (2015) 673–680.
[13] U. Javed, K. Ramaiyan, C. Kreller, E. Brosha, R. Mukundan, A. Morozov, Using sensor arrays to decode $NO_x/NH_3/C_3H_8$ gas mixtures for automotive exhaust monitoring, Sens. Actuators B Chem. 264 (2018) 110–118.
[14] T. Ritter, G. Hagen, J. Lattus, R. Moos, Solid state mixed-potential sensors as direct conversion sensors for automotive catalysts, Sens. Actuators B Chem. 255 (2018) 3025–3032.
[15] Y. Sadaoka, M. Mori, Detection of VOC in air with a planar-type potentiometric gas sensor based on YSZ with a Pt electrode modified with TiO_2, Sens. Actuators B Chem. 248 (2017) 878–885.
[16] F. Liu, Y. Wang, B. Wang, X. Yang, Q. Wang, X. Liang, P. Sun, X. Chuai, Y. Wang, G. Lu, Stabilized zirconia-based mixed potential type sensors utilizing $MnNb_2O_6$ sensing electrode for detection of low-concentration SO_2, Sens. Actuators B Chem. 238 (2017) 1024–1031.
[17] F. Liu, C. Ma, X. Hao, C. Yang, H. Zhu, X. Liang, P. Sun, F. Liu, X. Chuai, G. Lu, Highly sensitive gas sensor based on stabilized zirconia and $CdMoO_4$ sensing electrode for detection of acetone, Sens. Actuators B Chem. 248 (2017) 9–18.
[18] M. Muralidharan, V. Anbarasu, A. Perumal, K. Sivakumar, Enhanced ferromagnetism in Cr doped $SrMoO_4$ scheelite structured compounds, J. Mater. Sci: Mater. Electron. 27 (2016) 2545–2556.
[19] S. Culver, F. Rabuffetti, S. Zhou, M. Mecklenburg, Y. Song, B. Melot, R. Brutchey, Low-temperature synthesis of $AMoO_4$ (A = Ca, Sr, Ba) scheelite nanocrystals, Chem. Mater. 25 (2013) 4129–4134.
[20] T. Thongtem, A. Phuruangrat, S. Thongtem, Characterization of $MMoO_4$ (M = Ba, Sr and Ca) with different morphologies prepared using a cyclic microwave radiation, Mater. Lett. 62 (2008) 454–457.
[21] T. Basiev, A. Sobol, Y. Voronko, P. Zverev, Spontaneous Raman spectroscopy of tungstate and molybdate crystals for Raman lasers, Opt. Mater. (Amst.) 15 (2000) 205–216.
[22] M. Yu, L. Jiang, H. Yang, Ultrathin nanosheets constructed $CoMoO_4$ porous flowers with high activity for electrocatalytic oxygen evolution, Chem. Commun. 51 (2015) 14361–14364.
[23] J. Wang, A. Liu, C. Wang, R. You, F. Liu, S. Li, Z. Yang, J. He, X. Yan, P. Sun, G. Lu, Solid state electrolyte type gas sensor using stabilized zirconia and $MTiO_3$ (M: Zn, Co and Ni)-SE for detection of low concentration of SO_2, Sens. Actuators B Chem. 296 (2019) 126644.
[24] H. Jin, Y. Huang, J. Jian, Sensing mechanism of the zirconia-based highly selective NO sensor by using a plate-like Cr_2O_3 sensing electrode, Sens. Actuators B Chem. 219 (2015) 112–118.
[25] X. Zhang, H. Kohler, M. Schwotzer, Y. Wu, U. Guth, Mixed-potential gas sensor with layered Au, Pt-YSZ electrode: investigating the sensing mechanism with steady state and dynamic electrochemical methods, Sens. Actuators B Chem. 252 (2017) 554–560.
[26] F. Garzon, R. Mukundan, E. Brosha, Solid-state mixed potential gas sensors: theory, experiments and challenges, Solid State Ion. 136-137 (2000) 633–638.
[27] N. Miura, T. Sato, S.A. Anggraini, H. Ikeda, S. Zhuiykov, A review of mixed-potential type zirconia-based gas sensors, Ionics 20 (2014) 901–925.
[28] P. Elumalai, V.V. Plashnitsa, T. Ueda, M. Hasei, N. Miura, Dependence of NO_2 sensitivity on thickness of oxide-sensing electrodes for mixed-potential-type sensor using stabilized zirconia, Ionics 13 (2007) 387–393.
[29] B. White, E. Traversa, E. Wachsmana, Investigation of La_2CuO_4/YSZ/Pt potentiometric NO_x sensors with electrochemical impedance spectroscopy, J. Electrochem. Soc. 155 (2008) J11–J16.